

pubs.acs.org/JPCC Article

# Ag@Au and Au@Ag Core-Shell Nanoparticles: Insights on the **Growth Process and Interactions with Small Molecules**

Luiz Henrique dos Santos, F. D. Kiss, A. C. Ferraz, and R. Miotto\*



Cite This: J. Phys. Chem. C 2024, 128, 10751-10760



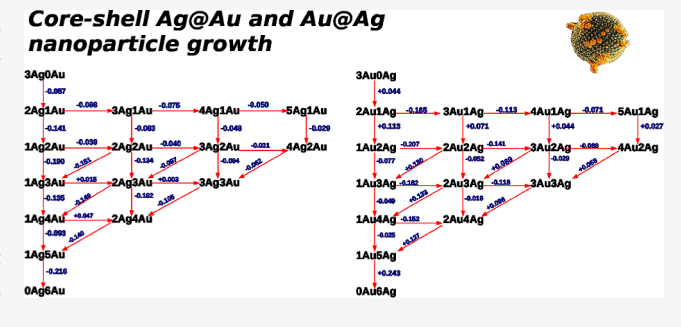
ACCESS I

Metrics & More

Article Recommendations

Supporting Information

ABSTRACT: In this investigation, we employed simulations and computational methodologies to examine pure silver and gold nanoparticles (NPs), alongside their core-shell configurations. Our research delved into, assessing the effects and adsorption tendencies of methanethiol molecules on diverse sites within these NPs. In our calculations, the effects of the inclusion of dispersion forces are analyzed. Structural analysis unveiled contractions in larger NPs and notable variations in adsorption energies across silver and gold surfaces. Furthermore, our study scrutinized not only the growth process but also the adsorption behavior of a model molecule within core-shell structures. We found that the



arrangement of metal layers within these structures significantly impacted the adsorption energies of methanethiol, closely resembling the behavior observed in the smaller pure gold NPs. Notably, even a single shell layer led to discernible changes in the electronic structure. Overall, our investigation underscored the profound influence of the NP size, composition, and arrangement on adsorption energies. Interestingly, introducing methanethiol molecules to larger-scale NPs exhibited minimal impact on the electronic structure despite the evident changes in adsorption behaviors.

## INTRODUCTION

Metal nanoparticles (NPs) exhibit optical and electronic properties influenced by their size and shape, distinct from those observed in bulk metals. This disparity has prompted widespread research into metallic NPs as fundamental components for nanoscale materials and devices. Gold and silver NPs, in particular, have undergone extensive exploration across various domains such as catalysis, the food industry, environmental conservation, fluorescence biosensors, glucose biosensors, nucleic acid-based biosensors, protein-based biosensors, drug delivery systems, and cancer therapies. 1-

Due to its high biocompatibility, chemical stability, and ease of surface modification, gold is often favored for biomedical applications. 1-3 Conversely, silver demonstrates higher plasmonic efficiency and superior magnetic enhancement in the visible range, making it more appealing for applications in optoelectronics, photovoltaics, and sensing. 1-3

Efforts have been directed toward synthesizing core-shell and alloy bimetallic NPs to combine these distinct properties. This approach aims to tailor the optical and catalytic properties of NPs, making the integrated system potentially valuable in diverse fields, such as taggants for security applications.<sup>3,4</sup>

The Au-Ag system is of particular interest because the surface plasmon resonance band might be tunable between  $\sim$ 520 nm for Au and  $\sim$ 410 nm for Ag.<sup>2–4</sup> These interesting physical and chemical properties are a result of the combination of the electronic properties of different metals and evolve new surface characteristics.

Besides its importance, most of the studies so far address AuAg alloy NPs properties and their growth process<sup>5-9</sup> in contrast to AuAg core-shell NPs. While experimental works rely on different techniques, such as aberration-corrected scanning transmission electron microscopy, Aberrationcorrected high-angle annular dark-field (HAADF), highresolution TEM, atomically resolved high-angle annular-darkfield scanning TEM, and energy-dispersive X-ray spectroscopy experiments,8 simulations are based on the doubly nudged elastic band algorithm coupled to empirical potentials<sup>5</sup> deep neural-network potential from small Au and Ag clusters using density functional theory (DFT), and molecular dynamics and molecular-dynamics and Monte Carlo simulations. In summary, these works agree that a multitude of geometric arrangements coexist within energy landscapes, potentially sharing similar energies and separated by transition barriers that can be overcome at room temperature.<sup>5</sup>

The adsorption process onto core-shell NPs significantly influences NPs' design and production. Methanethiol (SCH<sub>4</sub>) is notable for its atoms commonly engaged in surface

Received: May 8, 2024 Revised: June 7, 2024 Accepted: June 7, 2024 Published: June 15, 2024





interactions between organic structures of biological systems and metal NPs. Methanethiol serves as the simplest anchor sulfur group among  $\mathrm{CH_3}(\mathrm{CH_2})_n\mathrm{SH}$  ( $1 \le n \le 36$ ) systems used for growing self-assembled monolayers. Hence, this molecule offers an avenue to explore various adsorbed species under different conditions.

With a view to contribute to a better understanding of the surface properties of these complex systems, in this work we explore the stability, structural, and electronic properties nonalloy AuAg core—shell NPs and their interactions with small model molecules. The paper's structure is outlined as follows. In Methods, we present a concise description of our theoretical approach. Results and Discussion presents a discussion and comparison of our results regarding Au@Ag and Ag@Au core—shell NPs with existing theoretical and experimental works. In Conclusions, an investigation into the interaction between methanethiol and Ag, Au, Ag@Au, and Au@Ag NPs is provided. Finally, in Conclusions, a summary encapsulating the key findings and conclusions drawn from the study.

## METHODS

**Theoretical Modeling.** Noble-metal NPs can be synthesized in various shapes, including three-dimensional forms like spheres, cubes, octahedrons, dodecahedrons, and other polyhedrons. Additionally, two-dimensional structures such as triangles, squares, and other polygons have been reported. While some studies propose that stability is primarily determined by the number of atoms, 19–23 others suggest that both shape and arrangement can be influenced by the growth or synthesis method. 14,24–28

Metallic NPs typically adopt the face-centered cubic (FCC) or hexagonal close-packed crystal arrangements characteristic of metallic bonding, with a packing factor of 0.74 and 12 first neighbors.<sup>29</sup> For instance, in silver crystals, atoms are arranged in a FCC structure, and this is anticipated for silver-based NPs. However, small clusters are not constrained by crystalline periodicity, allowing for the observation of irregular solids such as icosahedral structures or asymmetric systems. 23,30,31 Additionally, they may form multiple twinned particles resembling decahedra or icosahedra, alongside various habit variations. Since our theoretical framework is based on DFT, a systematic study considering different reconstructions and possible segregation patterns is beyond our scope. These kinds of study are more suitable for empirical or mixed simulation approaches, such as the ones performed by Andolina et al.,7 Cruz and co-workers9 and Gromoff et al.8 and Gould and coworkers.<sup>5</sup> The diverse range of shapes and sizes possible for metallic NPs can render simulation attempts based on DFT impractical. To address this challenge, our study focuses solely on symmetric NPs, as discussed by Kiss et al.<sup>3</sup>

The modeling of cube-octahedral NPs with 147, 309, 561, and 923 atoms, corresponding to 3, 4, 5, and 6 atom layers, respectively, adopts an extended bulk structure based on FCC crystalline packing, tailored to achieve the desired geometries following the methodology detailed in Kiss et al.<sup>32</sup> These chosen NP sizes ensure adequate representation of both the structural and electronic NPs' properties.<sup>32</sup>

In our construction, these NPs resemble onions in their layered growth pattern, aligning with experimental observations by Maenosono and colleagues, which indicate controllable thickness of shell layers. For instance, the 561-atom NP comprises five layers. Core—shell NPs are created by replacing a layer of atoms. In this context, for a 561-atom NP, the

notation 3Ag@2Au indicates a NP consisting of two gold core layers and three silver shell layers. Figure 1 schematically illustrates the structure of the 3Ag@2Au NP.  $^{32}$ 

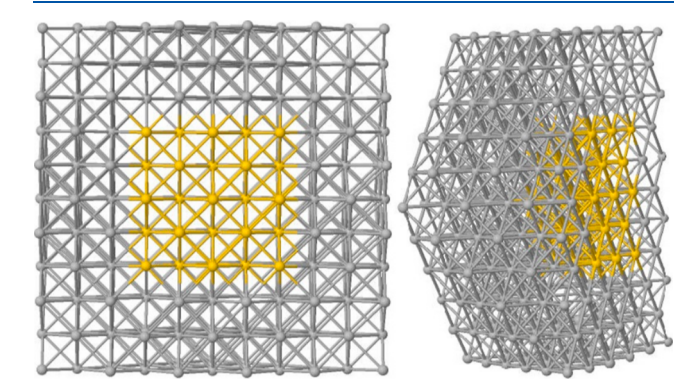


**Figure 1.** Schematic representation of a 561-atom NP is depicted, featuring two gold core layers (depicted as gold atoms) and three silver shell layers (depicted as gray atoms). This configuration is referred to as 3Ag@2Au for simplicity.

Our simulations are conducted utilizing the supercell scheme with a vacuum region exceeding 23 Å between the images of bare NPs. Ionic potentials are described using ultrasoft pseudopotentials, 34–36 while electron—electron exchange—correlation interactions are within the DFT framework employing the generalized gradient approximation by Perdew and Wang (PW91).<sup>37</sup> Spin polarization effects, as implemented in the Vienna Ab-initio Simulation Package, 38,39 are explicitly considered.

Single-particle orbitals are represented using a plane waves basis with energies up to 290 electronvolts (eV). Surface calculations adopt a 4  $\times$  4  $\times$  1 Monkhorst–Pack mesh, <sup>40</sup> whereas for NPs, only the  $\Gamma$  point is utilized. Altering the number of k-points or the basis set induces changes in total energies, atomic distances, and vibrational modes smaller than 0.05, 0.1, and 0.8%, respectively. Equilibrium positions for atoms are achieved when forces are below 10 meV/Å.

Dispersion forces, denoted as vdW, are incorporated using a pairwise force field proposed by Grimme. The  $C_6$  and  $R_0$  vdW parameters for gold and silver are 40.62/24.67 and 1.772/1.639, respectively. As indicated by Said and co-workers, the inclusion of dispersion forces using popular schemes such as the one adopted by us and the Tkatchenko-Scheffler method, among others, is system dependent, i.e., for some systems and properties, a given procedure gives better agreement with experimental results, while in other cases it is the other way round. Because the vdW approach by Grimme is among those more often used, our calculations rely on this scheme for deriving the dispersion forces.

The formation energy per atom ( $E_f$ ) and desorption energies are computed as indicated in Supporting Information, Section S1.

# ■ RESULTS AND DISCUSSION

Bare and Core-Shell NPs. In the initial phase of our study, we validated our model by computing the lattice parameter and the cohesive energy for both bulk gold and silver (Supporting Information, Section S2). Our calculations indicate that the inclusion of dispersion forces clearly leads to a better agreement between theoretical and experimental values, especially for cohesive energy. We have already shown<sup>32</sup> that

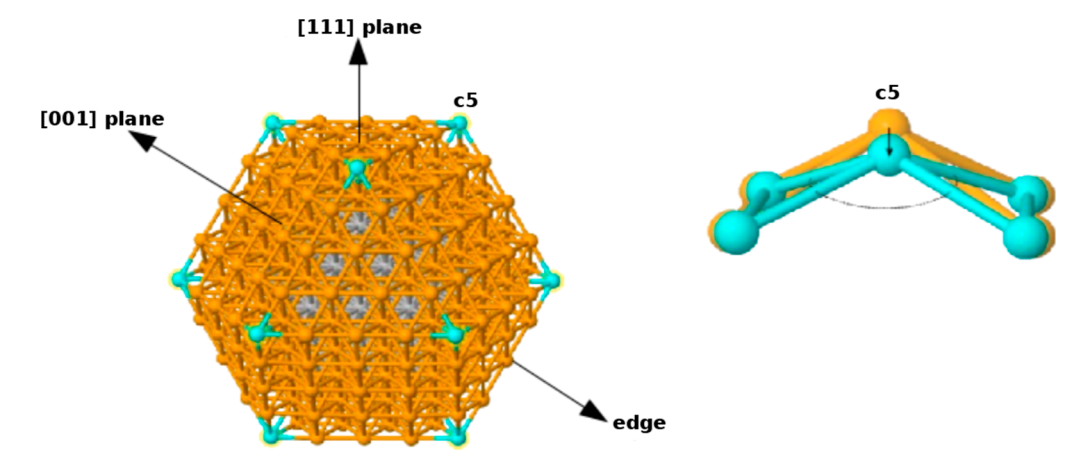


Figure 2. Schematic representation of the c5 coordination site, the [001] and [111] planes, and the edge formed by these two planes. In the detailed view, the characteristic bond angle of the C5 site is depicted. The color blue (gold) indicates unrelaxed (relaxed) positions.

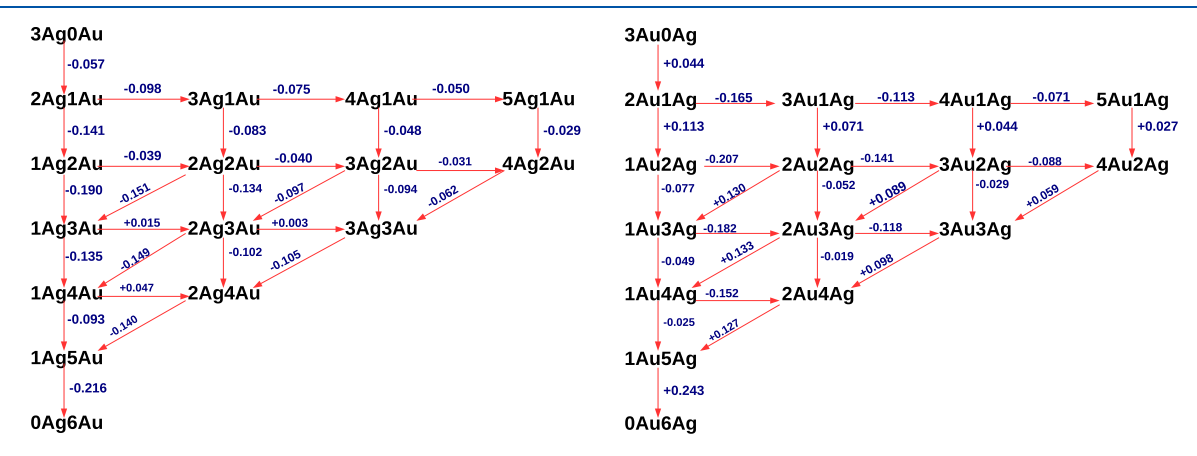


Figure 3. Energy difference in formation (without van der Waals forces), measured in eV, upon adsorption of a new shell atop an Ag (Au) core is demonstrated on the left (right) side of a 147 NP, representing 3 atomic layers. For instance, '3Ag1Au' designates a NP comprising a 3-layer Ag shell on a single layer of Au.

subsurface dislocations and relaxations are at least an order of magnitude smaller than those observed on the NP's surface and hence that the NP's properties are mainly mediated by its surface structural and electronic properties. Therefore, a proper description of the surface properties is a key point in our study of core—shell NPs and hence, the inclusion of dispersion forces is probably our best choice. Following this path, in subsequent discussions, calculations, including dispersion forces, are presented whenever similar trends are observed. However, both vdw and no-vdw results are explicitly discussed whenever discrepancies arise.

Changes in the structural properties of core—shell Au@Ag and Ag@Au in comparison to bare gold and silver NPs are considered by comparing bare gold and silver NPs as well as different Ag@Au and Au@Ag core—shell NPs comprising 147, 309, 561, and 923 atoms.

Our discussion on the structural properties primarily focuses on the c5 coordination site, the [001] and [111] planes, and the edges of these planes, as depicted in Figure 2, because these structures represent the NP under analysis, as discussed by Kiss et al.<sup>32</sup> Details of the structural analysis can be found in Supporting Information, Section S3.

The structural properties of all considered configurations exhibited consistent trends, regardless of whether dispersion forces were explicitly considered. Notably, significant contractions were consistently observed, particularly at the c5 site, with a proportional increase observed concerning the NP diameter. Specifically, among the examined systems, Au@Ag NPs demonstrated the most pronounced contractions compared to others (see Table S2 and Supporting Information, Section S3 for details).

Our calculations consistently indicated an increment in the distance between the central atom of the NP and the central atoms situated on the [111] and [001] planes, corresponding to an increase in NP sizes. Notably, these increments exceeded those observed in the unmodified [111] and [001] surfaces. Conversely, edge atoms within these planes exhibited closer proximity to the central atoms compared to the unrelaxed NP.

Collectively, the observed edge contractions, expansion of central plane atoms, and increase in  $\Delta c5 \angle$  strongly suggest a tendency of NPs to assume a more rounded configuration as additional layers are added. These findings align with observations from TEM images reported by Shankar et al. 44 and aberration-corrected HAADF by Cruz and co-workers. 9

In Figure 3, we illustrate the variation in formation energies, measured in eV, denoting energy gain, excluding van der Waals forces, upon adsorption of a new shell onto a 147 NP, representative of 3 atomic layers. Consistently, similar patterns are discernible when explicitly considering dispersion forces. Our investigation involves both Ag and Au cores coated with additional Au or Ag shell layers. For instance, '3Ag0Au'

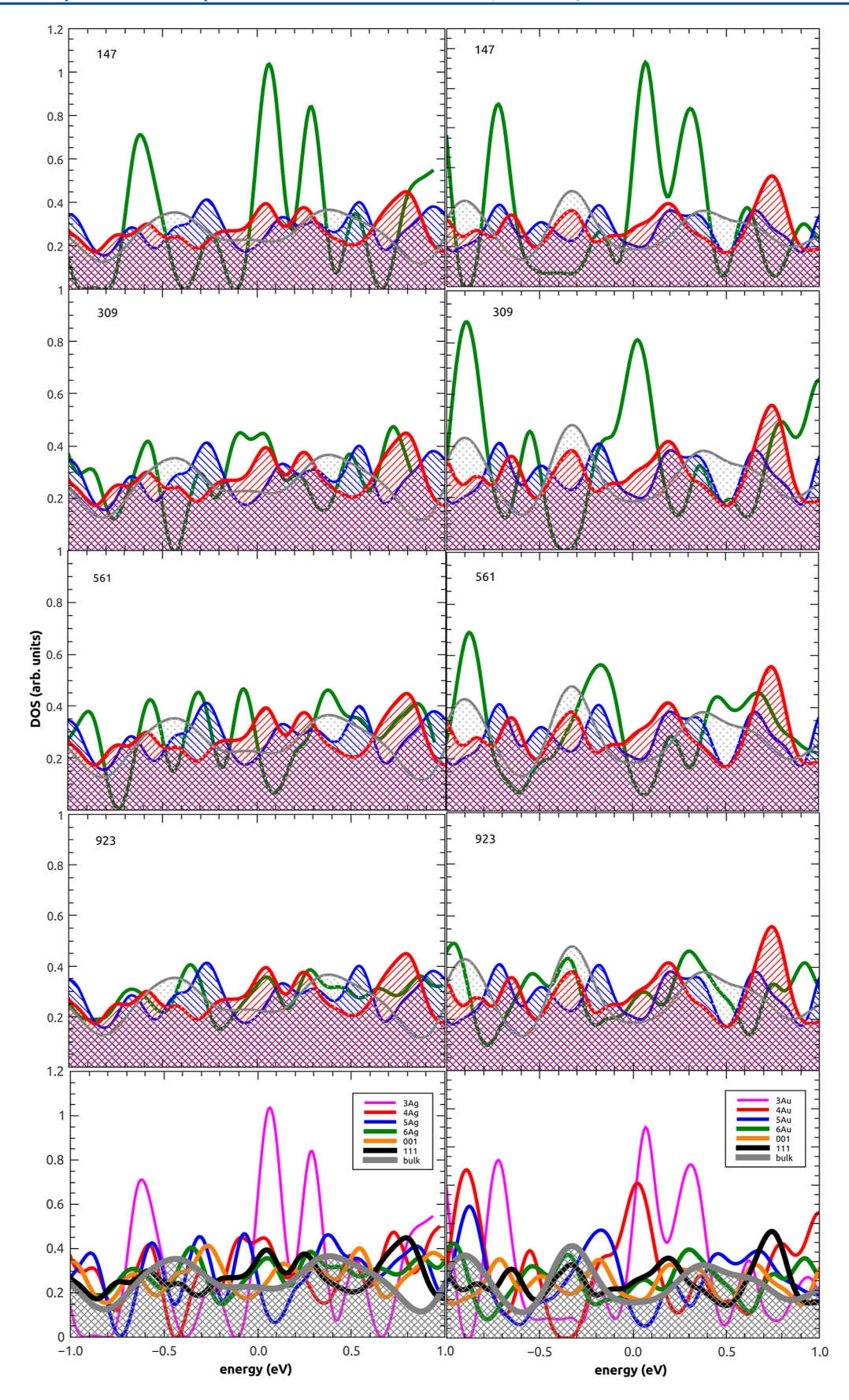


Figure 4. Upper panels:DOS for bare Ag (left) and Au (right) NPs. The quantity of atoms in each system is denoted in the top left corner of the respective panel. Lower panels: comparative analysis is presented between bare NPs, [001] and [111] surfaces, and the bulk DOS for Ag (left) and Au (right). The labels indicate the number of Ag and Au layers within a specific NP configuration. For instance, '4 Au' denotes a 309-atom NP comprising either 4 layers of silver or gold. These calculations do not incorporate dispersion forces.

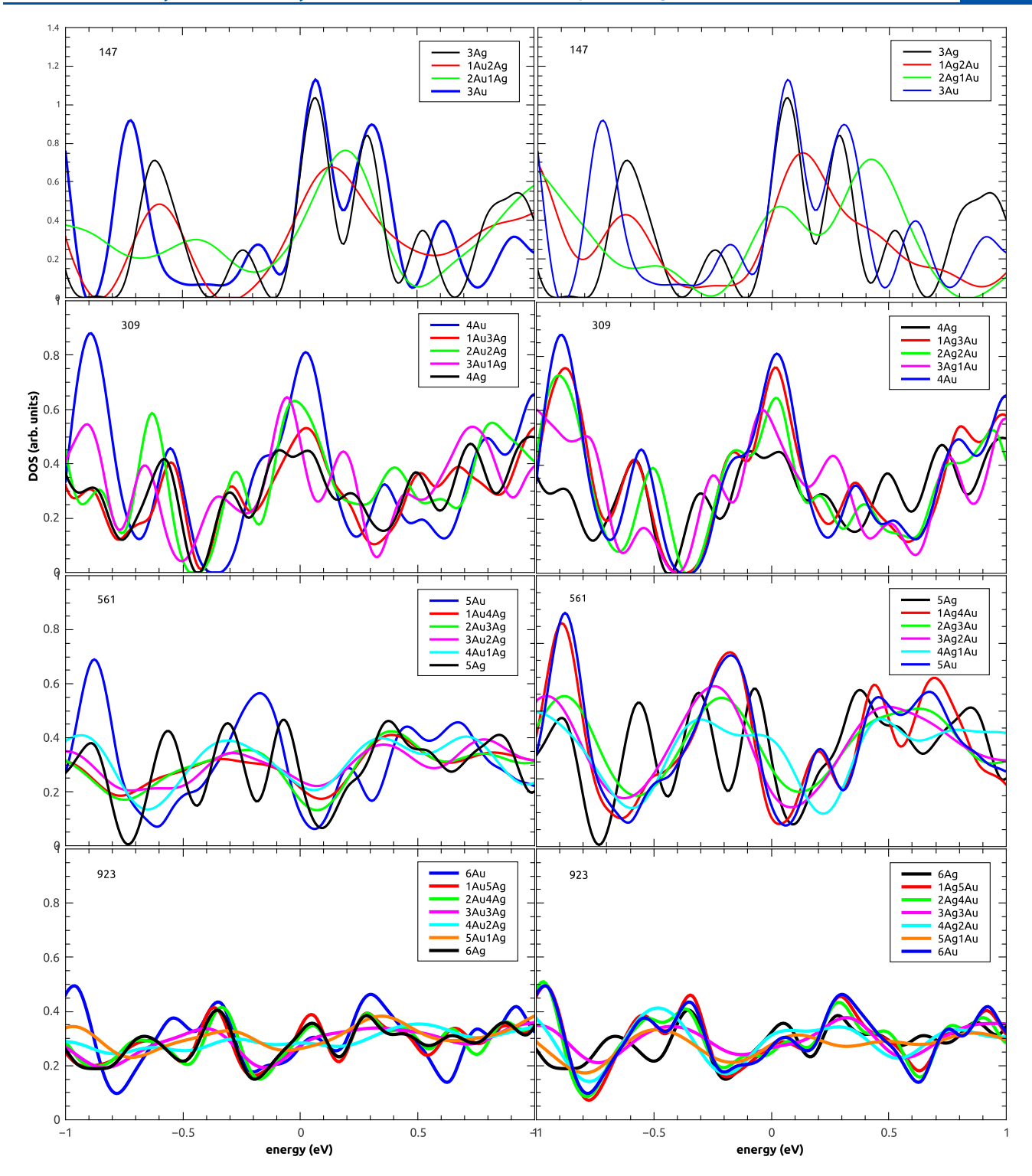


Figure 5. DOS for core—shell NPs, with the number of atoms in each system specified in the top left corner of the respective panel. For instance, '4Au2Ag' denotes a NP configuration comprising a 4-layer gold shell on a 2-layer silver core.

denotes a three-layer Ag core that can be covered by either one new Ag layer (4Ag0Au) or a new Au layer (3Ag1Au).

Our computational analyses indicate that initiating from an Au core, it is consistently less energetically favorable to encase it with one or more Ag shell layers compared to the addition of an extra Au shell layer. Conversely, in the case of a Ag core NP, the incorporation of Au shell layers consistently yields higher favorability than augmenting the size of a homonuclear Ag NP. This suggests that the growth of a Au shell layer on a Ag core

NP is more plausible than the growth of Ag shell layers on a Au core NP. Notably, similar outcomes were observed for larger NPs, including those with 306 and 561 atoms. Our observations are consistent with the experimental data and simulations by Andolina et al., Cruz and co-workers, and Gromoff et al. that overall suggested that gold surface segregation can be observed in vacuum while silver surface segregation is usually found in more reactive conditions.

Our simulations align with experimental evidence, indicating that the growth of Ag shells on Au cores necessitates a reducing agent to convert Ag(I) to Ag(0). Conversely, the growth of Au shells on Ag often occurs through galvanic exchange or transmetalation reactions, oxidizing Ag(0) to Ag(I) in solution while concurrently reducing Au(III) or Au(I) to Au(0).<sup>4</sup> Consequently, Ag@Au NPs exhibit a smooth Ag shell layer, as observed through various spectroscopic techniques by Güzel et al.<sup>45</sup> using ultraviolet—visible, reflection absorption infrared, and X-ray photoelectron spectroscopy.

Our findings also corroborate alternate synthetic pathways, such as the use of Neem (*Azadirachta indica*) leaf broth proposed by Shankar et al. <sup>44</sup> They found that, in a competitive process involving silver and gold ions, the reduction of gold ions is expedited, leading to silver not forming a uniform layer around core gold NPs but instead manifesting as smaller NPs that decorate them. It is crucial to note that our simulations do not encompass potential exchange or diffusion mechanisms, which may play a pivotal role in the growth process, as suggested by Shibata et al. <sup>46</sup>

The dissimilarities in the electronic structure between bare and core—shell NPs, as well as alterations due to the growth of new layer materials, are evaluated through a comparison of the density of states (DOS) of bulk Ag, bulk Au, bare [001], and [111] Au, and Ag surfaces with bare and core—shell NPs. To facilitate comparison, all DOS values are normalized by the system's electron count.

For the bare Ag and Au NPs depicted in Figure 4, our computations reveal that smaller systems (147 atoms) exhibit a distinct molecular character characterized by intense and localized peaks, influenced by the surface and bulk properties of the respective materials. As the NP size increases, the DOS approaches the surface and crystal characteristics. This observation is in line with our earlier findings for Ag NPs. However, an interesting distinction emerges: the decay of molecular characteristics on Au NPs is slower with increasing NP size compared with Ag NPs. This discrepancy signifies a lack of a universal rule dictating the NP size, where the transition from molecular to surface/crystal behavior occurs. Furthermore, the inclusion of dispersion forces does not significantly alter this overall trend.

Figure 5 displays the DOS for core—shell NPs. In subsequent discussions, the labeling of core—shell NPs follows a convention based on the counts of gold and silver layers. For instance, '4Au2Ag' designates a NP with a four-layer gold shell enveloping a two-layer silver core.

Our simulations reveal that the electronic structure of coreshell NPs represents a composite amalgamation of core and shell systems, showcasing intermediate states reminiscent of convolutions derived from the original DOS of bare Ag/Au NPs. Intriguingly, our observations indicate that even a single shell layer can induce such a modulation. This microscopic evidence suggests the amalgamation of electronic properties inherent in these materials, which elucidates the burgeoning interest in AuAg core—shell NPs.<sup>2–4</sup>

Consistently, our findings demonstrate that as the NP size increases the DOS increasingly resembles the characteristics of surface and crystal states. Notably, the inclusion of dispersion forces in our simulations does not significantly alter this overarching observation.

Adsorption on Core-Shell NPs. In our subsequent investigation, we discuss the interaction between methanethiol and Ag, Au, Ag@Au, and Au@Ag NPs. Despite its simplicity as

a molecule, methanethiol's composition involving carbon (C), sulfur (S), and hydrogen (H) atoms offers a diverse spectrum of potential adsorption processes commonly observed on metal surfaces. To explore this, we contrast the interaction of methanethiol with both bare Ag and Au NPs and surfaces against its interaction with Ag and Au core—shell NPs.

Figure 6 provides an overview of the available adsorption sites on the [111] and [001] faces of a NP. The quantity of

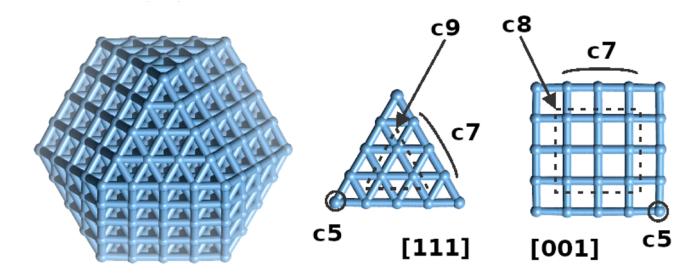


**Figure 6.** Schematic representation of distinct adsorption sites across various surfaces. Symbolized as cX, these designations represent specific adsorption sites characterized by different coordination numbers within a particular area. Enclosed by circles, brackets, squares, and triangles, the c5, c7, c8, and c9 sites, respectively, denote sites with varying coordination numbers.

available equivalent sites varies according to the NP's size, as discussed by Kiss et al.<sup>32</sup> This variability in available sites is a key issue in our examination of the adsorption behavior of methanethiol molecules.

As discussed in Supporting Information, Section S4, there is evidence suggesting a stronger interaction and greater affinity of methanethiol molecules for Au surfaces compared to those for Ag surfaces, regardless of the adsorption site or NP size. These findings highlight the importance of considering site-specific and size-dependent interactions between methanethiol and Ag/Au NP surfaces. The observed stronger affinity of methanethiol toward Au surfaces carries significant implications for catalytic and sensing applications that rely on NP surface properties.

Table 1 presents the adsorption energies  $(E_{\rm ads})$  in eV for methanethiol adsorption on the c5 site of NPs with 923 atoms. It includes both pure NPs (6Ag and 6Au) and core—shell NPs with various configurations (1Ag@5Au, 2Ag@4Au, 3Ag@3Au,

Table 1. Adsorption Energies ( $E_{\rm ads}$  in eV) for Methanethiol Adsorption on the c5 Site of Pure and Core—Shell NPs with 923 Atoms<sup>a</sup>

nanoparticle	$E_{ m ads}$ (eV)
1Ag@5Au	-0.5294
2Ag@4Au	-0.5278
3Ag@3Au	-0.5223
4Ag@2Au	-0.5203
5Ag@1Au	-0.5137
6Ag	-0.5203
1Au@5Ag	-0.4944
2Au@4Ag	-0.5173
3Au@3Ag	-0.5222
4Au@2Ag	-0.5242
5Au@1Ag	-0.5265
6Au	-0.5395

<sup>&</sup>lt;sup>a</sup>3Ag@2Au denotes a three-layered Ag shell on a 2 layers Au core NP.

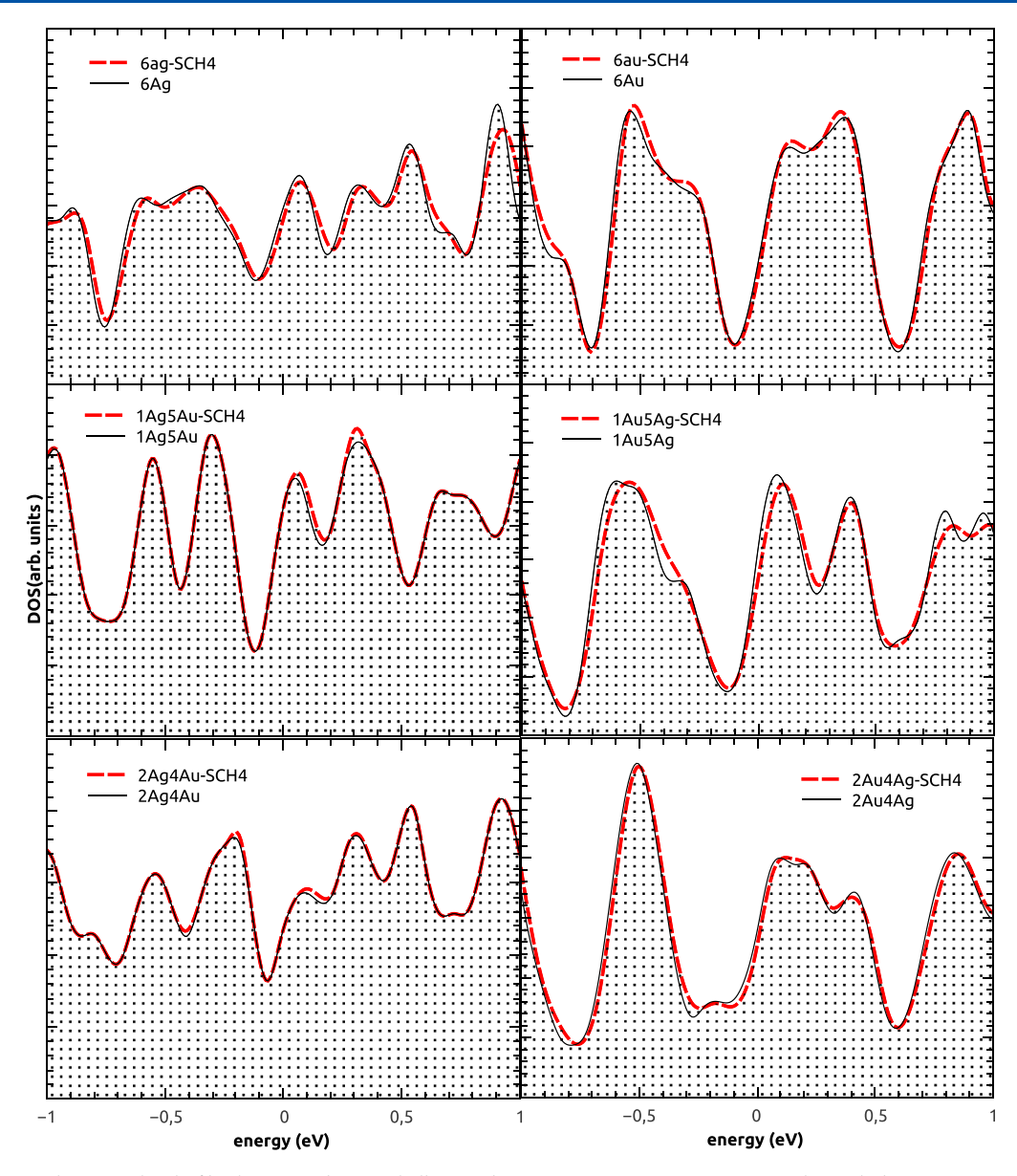


Figure 7. DOS near the Fermi level of both pure and core—shell Ag and Au NPs containing 923 atoms. It also includes a comparison with the DOS related to the adsorption of the methanethiol molecule (SCH<sub>4</sub>).

4Ag@2Au, 5Ag@1Au, 1Au@5Ag, 2Au@4Ag, 3Au@3Ag, 4Au@2Ag, and 5Au@1Ag).

The comparison between the adsorption energies of methanethiol on pure silver (Ag) and gold (Au) NPs and on core—shell configurations reveals noteworthy trends and potential correlations.

In the prior examination of pure Ag and Au NPs, a trend emerged showcasing a decrease in adsorption energies as the NP size increased. Specifically, larger Au NPs displayed higher adsorption energies compared to their Ag counterparts. This trend suggests that larger Au surfaces possess a stronger affinity for methanethiol molecules in comparison to larger Ag surfaces.

Analyzing the newly obtained data for core—shell NPs, several observations come to light. Configurations such as 1Ag@5Au, 2Ag@4Au, and 3Ag@3Au exhibited relatively higher adsorption energies, reminiscent of the higher adsorption energies observed for smaller pure Au NPs. Conversely, configurations with more Au layers and fewer Ag

layers displayed lower adsorption energies, resembling trends observed in larger pure Ag NPs.

This comparison implies a correlation between the arrangement of Ag and Au layers in core—shell configurations and the resulting adsorption energies. Specifically, core—shell configurations mimicking the surface characteristics of smaller pure Au NPs seem to exhibit enhanced methanethiol adsorption. This suggests the potential for tailored surface properties through strategic arrangements of Ag and Au layers in core—shell NPs, enabling control over the affinity for methanethiol.

Thus, the comparison highlights the influence of the NP size, composition, and arrangement on methanethiol adsorption. It hints at the possibility of engineering surface properties in core—shell NPs to achieve targeted adsorption behaviors, with potential implications in various catalytic and sensing applications.

It is important to highlight that our comparisons were made with particles containing the largest number of atoms in an attempt to consider only the region of crystalline regime, where the presence of the surface appears merely as a disturbance to the system, as discussed by Kiss et al.<sup>32</sup> Our calculations suggest that already from 561 atoms onward, the adsorption energies are practically equivalent among different sites, indicating that the NPs are already in the crystalline regime.

Upon methanethiol adsorption on core—shell structures, our investigation, detailed in Supporting Information, Section S5, unveils parallels with adsorptions on pure NPs. Notably, all Au–S bonds exhibit consistent shorter lengths compared to those of the Ag–S bonds. An intriguing observation arises concerning the adsorption energy, particularly notable at the c5 site, suggesting enhanced stability when the Ag(Au)–S bond length is shorter. Moreover, the binding energy, intensifying in absolute value and stability, aligns with a reduction in the Ag(Au)–S bond length from the c9 site to the c5 site across the core—shell surfaces. This trend mirrors changes observed in the Ag–Ag and Au–Au bonds (see Supporting Information, Section S5 for details).

The normalized DOS, characterizing pure and core—shell NPs composed of 923 atoms with mono- or bi-layered Au and Ag shells, is visually presented in Figure 7. Broadly, the introduction of methanethiol molecules onto larger-scale pure and core—shell Au and Ag NPs (with 561 and 923 atoms) shows minimal impact on their electronic structure. Any discernible effects remain subtle, exerting an insignificant influence.

## CONCLUSIONS

We investigated the structural, energetic, and electronic properties of pure Ag and Au NPs both on their own and when combined in core—shell structures. Our goal was to understand the implications arising from layering Au over Ag and Ag over Au, considering the dimensions of these structures. Additionally, we explored the dimensional influences through simulations, accounting for van der Waals interactions. The study extended to examine the adsorption of the methanethiol molecule (SCH<sub>4</sub>) on various coordination sites within these NPs. We modeled NPs in a cuboctahedral shape, ranging from 147 to 923 atoms, using first-principles calculations with DFT, employing ultrasoft pseudopotential methods.

Upon comparison with experimental values, minor variations in the calculated bulk lattice constants for silver and gold were observed, approximately 1.7 and 2.4%, respectively. However, discrepancies in cohesive energy were more pronounced, notably for gold. When dispersion forces were omitted, the deviation from experimental values for gold amounted to 19%, reducing to 1.8% when explicitly considered. Conversely, for silver, the deviation in cohesive energy from experimental values remained consistent regardless of considering dispersion forces.

We also looked at how the structure of bare NPs with added layers compares to that of core—shell Au@Ag and Ag@Au NPs. Our analysis covered different core—shell NP configurations comprising 147, 309, 561, and 923 atoms. Particularly, we focused on the c5 coordination site, the [001] and [111] planes, and their edges, observing consistent structural trends across all configurations, regardless of explicitly considering dispersion forces.

We found that larger NP sizes exhibited contractions, particularly at the c5 site, with Au@Ag NPs displaying the most pronounced contractions. The sum of angles involving

the c5 atom showed a positive correlation with the NP size, reflecting the composition of the surface shell layer. Notably, as the number of layers increased, the system converged toward the angle of the bare NP. In other words, adding layers tended to make larger NPs shrink slightly in certain areas while also increasing the angles between their atoms, resembling those of bare NPs

Our findings showed that it is generally easier to add gold layers onto silver cores than the other way around, which was consistent across different NP sizes, aligning with previous experimental data and simulations for AuAg alloy NPs by Andolina et al., Cruz and co-workers, and Gromoff et al., that overall suggested that gold surface segregation can be observed in vacuum while silver surface segregation is usually found in more reactive conditions.

Regarding adsorption energies, we found distinct variations across different adsorption sites for both Ag and Au NPs. In summary, Au surfaces exhibited stronger interactions and higher affinities for methanethiol molecules compared to Ag surfaces, regardless of the NP size or adsorption site.

Moreover, the comparison between different core—shell configurations indicated a correlation between the arrangement of Ag and Au layers and the resulting adsorption energies. Configurations resembling smaller pure Au NPs displayed enhanced methanethiol adsorption, suggesting the potential for tailored surface properties in the core—shell NPs.

It is also important to mention that, when compared to our previous investigations,<sup>32,47</sup> the inclusion of spin polarization effects did not change the observed trends. Although spin polarization effects were observed even for small Ag NPs,<sup>48</sup> spin polarization effects are not expected to play a crucial role, mainly because the properties investigated are not directly correlated to the system's magnetic properties.

Our simulations also provided insights into the electronic structure, showing that larger NPs exhibited characteristics akin to the surface and crystal states. Interestingly, even a single shell layer induced alterations, signifying the amalgamation of electronic properties in these materials.

Additionally, adding methanethiol molecules did not significantly change the electronic properties of the NPs.

In summary, our study provides detailed insights into how adding layers to NPs changes their properties and interactions with other molecules.

# ASSOCIATED CONTENT

## Supporting Information

The Supporting Information is available free of charge at https://pubs.acs.org/doi/10.1021/acs.jpcc.4c03044.

Theoretical modeling details, gold and silver crystals structural parameters, bare surfaces and core—shell NPs structure details and data, adsorption on bare NP details and data, and adsorption on core—shell NP details and data (PDF)

## AUTHOR INFORMATION

# **Corresponding Author**

R. Miotto — Centro de Ciências Naturais e Humanas, Universidade Federal do ABC, CEP 09210-580 Santo André, São Paulo, Brazil; orcid.org/0000-0001-5837-2569; Email: ronei.miotto@ufabc.edu.br

#### Authors

- Luiz Henrique dos Santos Instituto de Física da Universidade de São Paulo, CEP 05315-970 São Paulo, Brazil
- F. D. Kiss Instituto de Física da Universidade de São Paulo, CEP 05315-970 São Paulo, Brazil
- A. C. Ferraz Instituto de Física da Universidade de São Paulo, CEP 05315-970 São Paulo, Brazil

Complete contact information is available at: https://pubs.acs.org/10.1021/acs.jpcc.4c03044

#### **Funding**

The Article Processing Charge for the publication of this research was funded by the Coordination for the Improvement of Higher Education Personnel - CAPES (ROR identifier: 00x0ma614).

#### Notes

The authors declare no competing financial interest.

#### REFERENCES

- (1) Majdalawieh, A.; Kanan, M. C.; El-Kadri, O.; Kanan, S. M. Recent Advances in Gold and Silver Nanoparticles: Synthesis and Applications. *J. Nanosci. Nanotechnol.* **2014**, *14*, 4757–4780.
- (2) Hada, A.-m.; Potara, M.; Suarasan, S.; Vulpoi, A.; Nagy-Simon, T.; Licarete, E.; Astilean, S. Fabrication of gold—silver core—shell nanoparticles for performing as ultrabright SERS-nanotags inside human ovarian cancer cells. *Nanotechnology* **2019**, *30*, 315701.
- (3) Huang, Z.; Meng, G.; Hu, X.; Pan, Q.; Huo, D.; Zhou, H.; Ke, Y.; Wu, N. Plasmon-tunable Au@Ag core-shell spiky nanoparticles for surface-enhanced Raman scattering. *Nano Res.* **2019**, *12*, 449–455.
- (4) Shore, M. S.; Wang, J.; Johnston-Peck, A. C.; Oldenburg, A. L.; Tracy, J. B. Synthesis of Au(Core)/Ag(Shell) nanoparticles and their conversion to AuAg alloy nanoparticles. *Small* **2011**, *7*, 230–234.
- (5) Gould, A. L.; Rossi, K.; Catlow, C. R. A.; Baletto, F.; Logsdail, A. J. Controlling Structural Transitions in AuAg Nanoparticles through Precise Compositional Design. *J. Phys. Chem. Lett.* **2016**, *7*, 4414–4419.
- (6) Foster, D. M.; Ferrando, R.; Palmer, R. E. Experimental determination of the energy difference between competing isomers of deposited, size-selected gold nanoclusters. *Nat. Commun.* **2018**, *9*, 1222
- (7) Andolina, C. M.; Bon, M.; Passerone, D.; Saidi, W. A. Robust, Multi-Length-Scale, Machine Learning Potential for Ag–Au Bimetallic Alloys from Clusters to Bulk Materials. *J. Phys. Chem. C* **2021**, 125, 17438–17447.
- (8) Gromoff, Q.; Benzo, P.; Saidi, W. A.; Andolina, C. M.; Casanove, M.-J.; Hungria, T.; Barre, S.; Benoit, M.; Lam, J. Exploring the formation of gold/silver nanoalloys with gas-phase synthesis and machine-learning assisted simulations. *Nanoscale* **2024**, *16*, 384–393.
- (9) Mendoza-Cruz, R.; Palomares-Báez, J. P.; López-López, S. M.; Montejano-Carrizales, J. M.; Rodríguez López, J. L.; José Yacamán, M.; Bazán-Díaz, L. Experimental High-Resolution Observation of the Truncated Double-Icosahedron Structure: A Stable Twinned Shell in Alloyed Au—Ag Core@Shell Nanoparticles. *Nano Lett.* **2024**, 24, 4072—4081.
- (10) Dykman, L. A.; Bogatyrev, V. A. Gold nanoparticles: preparation, functionalisation and applications in biochemistry and immunochemistry. *Russ. Chem. Rev.* **2007**, *76*, 181–194.
- (11) Petroski, J.; Chou, M.; Creutz, C. The coordination chemistry of gold surfaces: Formation and far-infrared spectra of alkanethiolate-capped gold nanoparticles. *J. Organomet. Chem.* **2009**, *694*, 1138–1143.
- (12) Meyer, J.; Bredow, T.; Tegenkamp, C.; Pfnur, H. Thiol and thiolate bond formation of ferrocene-1,1-dithiol to a Ag(111) surface. *J. Chem. Phys.* **2006**, *125*, 194705.

- (13) Vericat, C.; Vela, M. E.; Benitez, G.; Carro, P.; Salvarezza, R. C. Self-assembled monolayers of thiols and dithiols on gold: new challenges for a well-known system. *Chem. Soc. Rev.* **2010**, *39*, 1805.
- (14) Akhavan, O. Silver nanocube crystals on titanium nitride buffer layer. *J. Phys. D: Appl. Phys.* **2009**, 42, 105305.
- (15) Martin, T. P. Shells of atoms. Phys. Rep. 1996, 273, 199-241.
- (16) Roduner, E. Size matters: why nanomaterials are different. *Chem. Soc. Rev.* **2006**, *35*, 583–592.
- (17) Pal, S.; Tak, Y. K.; Song, J. M. Does the Antibacterial Activity of Silver Nanoparticles Depend on the Shape of the Nanoparticle? A Study of the Gram-Negative Bacterium Escherichia coli. *Appl. Environ. Microbiol.* **2007**, *73*, 1712–1720.
- (18) Mock, J. J.; Barbic, M.; Smith, D. R.; Schultz, D. A.; Schultz, S. Shape effects in plasmon resonance of individual colloidal silver nanoparticles. *J. Chem. Phys.* **2002**, *116*, 6755–6759.
- (19) Jennison, D. R.; Schultz, P. A.; Sears, M. P. Ab initio calculations of Ru, Pd, and Ag cluster structure with 55, 135, and 140 atoms. *J. Chem. Phys.* 1997, 106, 1856–1862.
- (20) Blom, M. N.; Schooss, D.; Stairs, J.; Kappes, M. M. Experimental structure determination of silver cluster ions (Agn +,19≤n≤79). *J. Chem. Phys.* **2006**, 124, 244308.
- (21) Doye, J. P. K.; Wales, D. J. Global minima for transition metal clusters described by Sutton-Chen potentials. *New J. Chem.* **1998**, 22, 733–744.
- (22) Häkkinen, H.; Moseler, M.; Kostko, O.; Morgner, N.; Hoffmann, M. A.; Issendorff, B. v. Symmetry and Electronic Structure of Noble-Metal Nanoparticles and the Role of Relativity. *Phys. Rev. Lett.* **2004**, *93*, 93401.
- (23) Poteau, R.; Spiegelmann, F. Structural properties of sodium microclusters (n = 4–34) using a Monte Carlo growth method. *J. Chem. Phys.* **1993**, 98, 6540–6557.
- (24) Burda, C.; Chen, X.; Narayanan, R.; El-Sayed, M. a. Chemistry and properties of nanocrystals of different shapes. *Chem. Rev.* **2005**, 105, 1025–1102.
- (25) Sun, Y.; Xia, Y. Shape-Controlled Synthesis of Gold and Silver Nanoparticles. *Science* **2002**, 298, 2176–2179.
- (26) Koski, K. J.; Kamp, N. M.; Smith, R. K.; Kunz, M.; Knight, J. K.; Alivisatos, A. P. Structural distortions in  $5-10 \sim \text{nm}$  silver nanoparticles under high pressure. *Phys. Rev. B* **2008**, *78*, 165410.
- (27) Kan, C.-X.; Zhu, J.-J.; Zhu, X.-G. Silver nanostructures with well-controlled shapes: synthesis, characterization and growth mechanisms. *J. Phys. D: Appl. Phys.* **2008**, *41* (15), 155304.
- (28) Maliszewska, I.; Szewczyk, K.; Waszak, K. Biological synthesis of silver nanoparticles. *J. Phys.: Conf. Ser.* **2009**, 146, 012025.
- (29) Kittel, C. Introduction to Solid State Physics; John Wiley and Sons: New York, 2004.
- (30) Poteau, R.; Heully, J.-L.; Spiegelmann, F. Structure, stability, and vibrational properties of small silver cluster. *Zeitschrift fur Physik D Atoms, Molecules and Clusters* **1997**, *40*, 479–482.
- (31) Huda, M. N.; Ray, A. K. Electronic structures and magic numbers of small silver clusters: A many-body perturbation-theoretic study. *Phys. Rev. A* **2003**, *67*, 013201.
- (32) Kiss, F. D.; Miotto, R.; Ferraz, A. C. Size effects on silver nanoparticles' properties. *Nanotechnology* **2011**, *22*, 275708.
- (33) Maenosono, S.; Lee, J.; Dao, A. T. N.; Mott, D. Peak shape analysis of Ag 3d core-level X-ray photoelectron spectra of Au@Ag core-shell nanoparticles using an asymmetric Gaussian-Lorentzian mixed function. *Surf. Interface Anal.* **2012**, *44*, 1611–1614.
- (34) Vanderbilt, D. Optimally smooth norm-conserving pseudopotentials. *Phys. Rev. B* **1985**, 32, 8412–8415.
- (35) Vanderbilt, D. Soft self-consistent pseudopotentials in a generalized eigenvalue formalism. *Phys. Rev. B* **1990**, *41*, 7892–7895.
- (36) Kresse, G.; Joubert, D. From ultrasoft pseudopotentials to the projector augmented-wave method. *Phys. Rev. B* **1999**, *59*, 1758–1775.
- (37) Perdew, J. P.; Chevary, J. A.; Vosko, S. H.; Jackson, K. A.; Pederson, M. R.; Singh, D. J.; Fiolhais, C. Atoms, molecules, solids, and surfaces: Applications of the generalized gradient approximation for exchange and correlation. *Phys. Rev. B* **1992**, *46*, 6671–6687.

- (38) Kresse, G.; Furthmüller, J. Efficient iterative schemes for ab initio total-energy calculations using a plane-wave basis set. *Phys. Rev.* B **1996**, *54*, 11169–11186.
- (39) Kresse, G.; Furthmüller, J. Efficiency of ab-initio total energy calculations for metals and semiconductors using a plane-wave basis set. *Comput. Mater. Sci.* **1996**, *6*, 15–50.
- (40) Monkhorst, H. J.; Pack, J. D. Special points for Brillouin-zone integrations. *Phys. Rev. B* **1976**, *13*, 5188–5192.
- (41) Grimme, S. Semiempirical GGA-type density functional constructed with a long-range dispersion correction. *J. Comput. Chem.* **2006**, 27, 1787–1799.
- (42) Al-Saidi, W. A.; Voora, V. K.; Jordan, K. D. An Assessment of the vdW-TS Method for Extended Systems. *J. Chem. Theory Comput.* **2012**, *8*, 1503–1513.
- (43) Tkatchenko, A.; Scheffler, M. Accurate Molecular Van Der Waals Interactions from Ground-State Electron Density and Free-Atom Reference Data. *Phys. Rev. Lett.* **2009**, *102*, 073005.
- (44) Shankar, S. S.; Rai, A.; Ahmad, A.; Sastry, M. Rapid synthesis of Au, Ag, and bimetallic Au core-Ag shell nanoparticles using Neem (Azadirachta indica) leaf broth. *J. Colloid Interface Sci.* **2004**, 275, 496–502.
- (45) Güzel, R.; Üstündağ, Z.; Ekşi, H.; Keskin, S.; Taner, B.; Durgun, Z. G.; Turan, A. A. I.; Solak, A. O. Effect of Au and Au@Ag core-shell nanoparticles on the SERS of bridging organic molecules. *J. Colloid Interface Sci.* **2010**, *351*, 35–42.
- (46) Shibata, T.; Bunker, B. A.; Zhang, Z.; Meisel, D.; Vardeman, C. F.; Gezelter, J. D. Size-Dependent Spontaneous Alloying of Au-Ag Nanoparticles. *J. Am. Chem. Soc.* **2002**, *124*, 11989–11996.
- (47) Miotto, R.; Kiss, F. D.; Ferraz, A. C. Changes in a nanoparticle's spectroscopic signal mediated by the local environment. *Nanotechnology* **2012**, 23, 485202.
- (48) Li, W.-H.; Lee, C.-H. Complex Magnetic Nanostructures; Springer International Publishing: Cham, 2017; pp 195–224.